

Decision making and uncertainty: Bayesian analysis of potential flood heights

Steven M. Manson ¹
Samuel J. Ratick ²
Andrew R. Solow ³

1 – Department of Geography
University of Minnesota
414 Social Science Building
267 19th Avenue South
Minneapolis, MN 55455

2 - Graduate School of Geography, and
The George Perkins Marsh Institute
Clark University
Worcester MA 01610-1477 USA

3 - Woods Hole Oceanographic Institution
Marine Policy Center
Crowell House, Mail Stop 41
Woods Hole MA 02543-1138 USA

Abstract - This paper provides a case study of a method to estimate the value of additional information, before its acquisition, to aid decision making in the face of uncertainty. The approach employs conditional simulation in a Monte Carlo framework to conduct a Bayesian assessment of the value of information in an explicitly spatial setting. This paper demonstrates the procedure as applied by a hypothetical decision maker concerned with coastal flood control where flood damage is dependent on the spatial distribution of elevation. A set of known survey points provides the decision maker with limited knowledge of elevation. The method explored in the paper allows the decision maker to ascertain the potential value of additional survey information in terms of its ability to reduce uncertainty about flood damage.

Keywords: Bayesian, conditional simulation, spatial decision making, flooding

Citation: Manson, S. M., S. J. Ratick and A. R. Solow (2002). Decision making and uncertainty: Bayesian analysis of potential flood heights. *Geographical Analysis* 34(2): 112-129.

PREPRESS VERSION

1 Introduction

Floods are one of the most common hazards faced by humans. The risk posed by flooding has become more significant in light of global environmental change. In particular, there is general agreement in the global change research community on the potential for an increase in the mean global temperature resulting in subsequent sea level rise (Wigley and Raper 1992). In addition to higher flood heights, a raised base water level accelerates beach erosion, increases flood frequency, and affords greater energy to waves and storm surges (Leatherman 1992).

Decision makers, ranging from individuals to national governments, must decide among a variety of mitigative and adaptive responses to flooding. This decision process is fraught with uncertainty stemming from scientific disagreement over the magnitude of sea-level rise, the changing nature of coastal landform processes, and insufficient knowledge of the topography of susceptible areas. Uncertainty affects how decision makers plan for flooding given that flood alleviation measures have different social and economic costs. Decision makers must, therefore, often acquire additional information in order to reduce uncertainty and better understand potential flood processes.

This study is an outgrowth of a project sponsored by the National Oceanic and Atmospheric Administration (NOAA) to examine the role of uncertainty about topography in understanding the potential effects of sea-level rise (Ratick et al. 1994). The present research examines decision making about flooding by joining geographic information system (GIS) methods and spatial analysis to implement Bayesian decision theory. The paper offers a case study in which a hypothetical decision maker employs Bayesian analysis in a real world setting.

Section 2 describes the Bayesian procedure and its underlying theoretical framework. This section first describes the relationship between Bayesian decision theory and geostatistics. It then describes a Monte Carlo process that employs conditional simulation to model topographic uncertainty in a GIS setting.

Section 3 demonstrates the Bayesian procedure described in section 2. This section presents a situation in which a hypothetical decision maker with limited information models uncertainty in flood processes and ascertains the potential value of further information. A hypothetical but representative case study is then developed based on an actual dataset. This allows for a realistic demonstration of the procedure and enables verification of its performance.

Section 4 evaluates how well the procedure works as an aid to decision making. It first compares model results to actual elevation and flood data and then demonstrates how a decision maker may successfully use the procedure in both a generic Bayesian sense and in a more spatially explicit manner.

Section 5 concludes with key findings and future research directions.

2 Uncertainty Assessment

Uncertainty is a “fundamental dimension” of decision making analogous to time or space (Chrisman 1991: 167) and frequently is associated with source data and its display and manipulation (Goodchild et al. 1994). Often digital elevation models (DEM) are used to identify regions that are prone to flooding. However, the accuracy of such evaluations can be affected by errors in data collection, digital storage, and the means used to interpolate elevation in the DEM (Heuvelink 1993). This study treats these errors as the key source of uncertainty faced by the decision maker, although there are certainly other sources such as cognitive bias or epistemic failure.

Combining GIS and spatial analysis, particularly geostatistics, is a valuable means of dealing with uncertainty (Journal 1996). Uncertainty is considered through a Bayesian decision analysis framework implemented with a Monte Carlo conditional simulation procedure in a GIS setting. This research is a valuable addition to approaches in hydrological and flood modeling that accommodate uncertainty, such as entropy models (Husain 1990), simulation methods (Melching and Anmangandla 1992), and statistical models (Rosbjerg and Madsen 1995).

2.1 Bayesian Decision Analysis

Bayesian decision analysis is manifest over a diverse and mature body of literature (Berger 1986; Cyert and DeGroot 1987). Under Bayesian decision analysis, a decision maker can make informed decisions about a future event by combining prior probability with current observations to create a posterior probability. This analysis applies to situations where error or uncertainty is not randomly distributed but instead jointly distributed. This may be expressed as a Bayesian decision function:

$$R(\xi, \delta) = \int \int_{\Omega, x} L[\phi, \delta(x)] f(x | \phi) \xi(\phi) dx d\phi \quad (1)$$

where one evaluates the expected risk, $R(\xi, \delta)$ with respect to prior distribution ξ for a given decision function within parameter space Ω , loss function L , and a family of conditional density functions $f(x | \phi)$ for a set of observations x . The posterior distribution of ϕ is conditioned by given observed values $X = x$.

Bayesian decision analysis extends successfully into geostatistics. One may estimate the value of additional observations, before acquisition, to the understanding of the spatial nature of a DEM terrain surface (Solow and Ratick 1994). Estimating the value of potential observations is possible if there exists a satisfactory approximation of the topographical nature of the surface. A Bayesian function

$$E(E^*(x, U) | x) = \int E^*(x, u) f(u | x) du \quad (2)$$

substitutes the estimated value E of a set of additional observations U for the extent to which the expected risk ($R(\xi, \delta)$ in Equation 1) is reduced given a loss function based on elevation ($L[\phi, \delta(x)]$ in Equation 1). Known survey points x give a prior distribution ($\xi(\phi)$ in Equation 1) within a parameter space defined as elevation (Ω in Equation 1). Finally, for the conditional density function $f(x | \phi)$ in Equation 1, Equation 2 substitutes function f of additional survey points u given x .

Equation 2 translates into a GIS-geostatistical setting as follows:

$$E(E^*(x, U) | x) = \sum_{j=1}^K E^*(x, u_x^j) / K \quad (3)$$

whereby the decision maker can estimate the benefit of additional sample locations U based on the current understanding of the terrain surface derived from a set of known survey points x and $j = 1, 2, \dots, K$ sets of potential additional locations u . As the same process underlies the creation of the terrain surface and x , a decision maker may take a set of additional points u that approximates what he or she expects in reality.

2.2 Implementation

Equation 3 is implemented as a Monte Carlo estimation procedure in a GIS-geostatistics framework. The computational form of $f(u|x)$ in Equation 2 that determines E in Equation 3 lies in conditional simulation. Conditional simulation is based on kriging, a technique that employs a *semi-variogram* (denoted γ and generally termed a variogram) developed directly from sample data to model the statistical weight of sample points for interpolation (Isaaks and Srivastava 1989). Kriging is considered more fully in section 3.2. Conditional simulation creates a surface, or realization, by using a surface estimated by kriging and adding to it a probabilistic estimate of error derived from the kriging variance (Journel 1996). Each simulated surface is ‘conditioned’ by being constrained by the sample points.

As a means of dealing with uncertainty in the context described here, conditional simulation offers advantages over other interpolation techniques such as trend surface analysis, Thiessen tessellation, distance-weighted averaging, spectral analysis, splines, and triangulated irregular networks (see Burrough and McDonnell 1998; Eastman 1999). Conditional simulation ties terrain to underlying topographical processes by recognizing the variability masked by interpolation and remedying this by reintroducing the kriging variance. Conditional simulation has several other advantages: 1) interpolated values can lie beyond the range of samples upon which they are based; 2) it provides varying plausible realizations necessary for Monte Carlo analysis; 3) consideration of anisotropic spatial dependency based upon statistical distance combined with global spatial trends; and 4) reduction of the redundancy caused by clustering in sample points (Deutsch and Journel 1992).

A decision maker implements the Bayesian decision function expressed in Equation 3 as the three-part Monte Carlo estimation procedure shown in Figure 1.

Insert Figure 1 here

Step One of the procedure: a) draws a sample x ; b) defines a variogram γ to fit these sample locations in order to characterize the terrain surface; and c) krigs surface **A** to act as the base for the remainder of the estimation procedure. Step Two is the nested Monte Carlo analysis proper whose constituent steps repeat. This part of the procedure: a) conditionally simulates a terrain surface **B** with known points x ; b) draws a set of additional points u from **B** that correspond to *potential* survey locations; and c) generates a second terrain surface **C** based on both the known points x and additional points u . Step Three simulates flooding in sets **B** and **C** of conditionally simulated realizations. It then remains to analyze the difference in flooding between sets **B** and **C** to estimate the value of information of the *potential* additional observations u .

3 Application

This section presents how a hypothetical decision maker uses the Bayesian procedure described in the previous section to model uncertainty in flood processes and ascertain the potential value of further information. The section begins with a description of the study site and data. It then introduces the hypothetical decision maker and the derivation of a representative example terrain from real data. The decision maker then applies the Bayesian procedure within the context of the approximation of the study site.

3.1 Study Site, Data, and Computational Setting

The study site, Point of Pines, is a small peninsular community several kilometers north of Boston, Massachusetts. Both the Atlantic Ocean and the Pines River border Point of Pines and

the community is therefore prone to riverine and storm surge flooding in addition to slow inundation due to rising sea level. The area is largely developed given its proximity to Boston and the ocean.

Figure 2 is a generalized elevation contour map of the study site derived from a surface \mathbf{R} kriged from several thousand locations (denoted r) surveyed by the US Army Corps. It is assumed that r will provide an error-free representation of reality (which is reasonable because the data was collected with ground-based optical techniques that ensure it is accurate to a maximum fifteen centimeter vertical RMS (USACE 1994)). Other possible means of gathering data for a DEM include use of global positioning system units, photogrammetry (e.g., from aerial photographs and satellite imagery), and newer techniques such as laser altimetry (Hill et al. 2000) and synthetic aperture radar interferometry (Dixon 1995). Figure 2 is inset with roads digitized from United States Geological Survey (USGS) 1:5000 scale digital black and white orthophotos taken April 1995.

Insert Figure 2 here

Anselin and Getis describe three degrees of integration between GIS and spatial analysis: 1) full integration; 2) closely-linked modules; and 3) use of import/export filters (1992: 23). The work described here is an example of the third kind as it was necessary to create custom applications for file conversion and data transformation. The bulk of data manipulation and analysis is in Idrisi, a raster based GIS (Eastman 1999). VarioWin performs variogram derivation (Panatier 1996). GSTAT is responsible for kriging and conditional simulation (Pebesma 1996).¹

The following describes the implementation of the nested Monte Carlo procedure using the Point of Pines case study data. It is important to note that throughout this analysis the only ‘real’ data values at the disposal of the decision maker are the elevations of the initial set of survey locations (x) chosen from the full set r . This provides the luxury of being able to compare the results of the nested Monte Carlo procedure to ‘reality,’ the surface \mathbf{R} kriged using the full set of r survey locations.

3.2 Primary Samples, Variogram Derivation, and Kriging

The Bayesian procedure begins with the decision maker sampling primary locations x from reality r (step 1a in Figure 1). One hundred samples were drawn from r , assuming that a reasonable minimum sample size (n_x) for x is between 50 to 100 observations (Burrough and McDonnell 1998: 137). This range is only a guide, however, and the ability to accurately interpolates elevation is the prime consideration. Fortunately, the r survey locations were originally chosen to balance spatial coverage vs. areal extent, terrain complexity (e.g., topographically significant phenomena such as ridge lines), and socially important factors such as house foundations. Any resultant clustering in r is minimized by a random stratified sample of r to obtain x (Figure 3). As noted above, any residual clustering is accommodated by kriging and conditional simulation. The values of x range from 0 to 4.57 m and have a mean of 2.65 m ($s^2 = 0.54$).

Insert Figure 3 here

VarioWin is used to derive a variogram γ from x (step 1b); the resultant variogram is an uncompounded spherical function determined to be self-consistent through cross-validation (see Panatier 1996). Use of the spherical model is consistent with other research that finds success in using similar ‘transitive’ variograms for landforms (Oliver and Webster 1986).

¹ The latest version of the Idrisi GIS contains GSTAT as an integrated module.

Underlying the variogram is the understanding that the spatial variation of any variable has three components: 1) a structural component; 2) a random spatially correlated component; and 3) spatially uncorrelated error. The first component is the average elevation of the study site. The variogram expresses the second component as a spatially dependent random variable. The statistical influence of γ declines (i.e., variability increases) at a rate described by the spherical model. The general north-by-northeast trend of the study site topography is described by an *anisotropy ratio* of a major axis oriented along the general trend and a perpendicular minor axis. The study site has a ratio of 0.7, creating an ellipse of statistical influence bearing 20 degrees (where 0 degrees = north). A search distance of 300 m limits the influence of distant points and the procedure simulates cells in the landscape at resolution of roughly 4.5 m².

The set of sample locations x and variogram γ characterize the study site. Surface **A** is kriged from the x samples to represent study site elevation (step 1c). Ordinary kriging is employed, as it is useful for interpolating from a sparse data set for a single, continuous variable. Universal kriging could also be used because it is more adept at accommodating a regional trend, as is often found with elevation. This is not the case with the study site, however, given that it is a peninsula and anisotropy accommodates the overriding landscape trend, directionality.

3.3 Monte Carlo Procedure

With the variogram γ , sample points x , and kriged surface **A** from step 1, the Monte Carlo component of the Bayesian procedure is implemented (step 2 in Figure 1). In step 2a, conditional simulation is used to create **B**, a set of 130 realizations from **A** and x that are varying, but statistically plausible, representations of the Point of Pines topography. The decision maker knows only the elevations of the x locations with ‘certainty,’ while the elevations of the potential u sample sites vary based on their resultant values in the **B** conditional simulations. The crux of the Monte Carlo procedure lies in determining, in a value of information sense, whether the decision maker should actually survey the u locations. This analysis is conducted for the case study scenario in the following section.

Before continuing, however, it is necessary to consider how the difference between series **B** and **C** is useful if no ‘new’ information is introduced when simulating the latter. The only difference between the two series lies in the use of additional points u that are derived from **B**. Since both series share identical sample locations x and variogram γ , **B** and **C** are reasonably expected to be statistically similar. Indeed, using conditional simulation for interpolation is defensible only in so far as it relies on realizations being equiprobable and statistically similar. As the number of individual realizations in the **B** and **C** series increases, the mean surface for these series decreases, where the each cell in a mean surface is the mean value for that location over a series of images. For a very large number of realizations, the mean surfaces for **B** and **C** would be almost identical to one another and to a kriged surface given shared underlying data and variogram.

The method works despite this statistical characteristic because it does not consider flooding in mean surfaces. It instead relies on flooding being a function of how proximal locations vary jointly within an equiprobable image. In other words, it is less a question of how elevation varies for a given cell over a series of images and more a question of how the cell’s elevation varies with respect to its neighbors in any one image. Addition of u to the simulation of series **C** has a distinct effect on the relative elevations of cell groups due to the manner in which conditional simulation treats initial observations. Section 4.3 explores this mechanism more fully. The ability to create varying surfaces in a manner similar to that used here makes

conditional simulation a prime choice for assessing probabilistic processes over space (USACE 1997).

In Step 2b, multiple sets of potential sample locations u are drawn from **B**. The number of additional points extracted from **B** varies, as a basic task for the analysis is to determine the number (n_u) of additional locations to survey. To evaluate this in the case study, a range of sample sizes for u were randomly sampled from **B** and evaluated (keeping in mind that **B** is simulated from variogram γ and sample points x). For the Point of Pines topography, less than 25 samples are too few and more than 600 do not yield significantly different results; therefore, 24 different sets of u from each of the 130 **B** realizations were used, ranging from 25 to 600 locations at 25 point intervals (i.e., $n_u = 25, 50, 75, \dots, 575, 600$).

In step 2c, a set of realizations **C**, result from conditional simulations based on sample locations x , u , and kriged surface **A** (or in other terms, variogram γ and points x give surface **A**). There are two chief results of the Monte Carlo procedure in step 2. The first is **B**, a set of 130 terrain realizations simulated from kriged surface **A** and x . The second is **C**, sets of 130 simulated terrains for each of the 24 sample sets of u (where $n_u = 25, 50, 75, \dots, 600$). There are therefore 24 sets of 130 realizations, for a total of 3120 surfaces in set **C** that are created from surface **A**, known locations x , and potential locations u .

3.4 Flooding

The two sets of realizations, **B** and **C**, are imported into GIS layers. Because the interest here is a general treatment of the value of additional information, flooding **B** and **C** only requires a simple sunken valley approach, which does not evaluate the effects of coastal erosion, subsidence, or storm surge (cf. Ostroff and Tucker 1992). The spatially explicit flooding procedure only inundates cells that have a route to the ocean lying entirely under the flood height. Each GIS layer (a topographic realization of the Point of Pines area) receives artificial sea-levels ranging from 0.3 m to 3.0 m, the latter being the height at which water overtops the bulk of the study site.

4 Findings

How well does the Bayesian procedure perform? This question may be answered in two ways. First, the simulated surfaces created by the procedure can be tested for their approximation to reality. Section 4.1 assesses how the conditionally simulated surfaces fare in regard to actual elevations and historical flooding patterns in Point of Pines. Second, the Bayesian analysis as such is conducted by determining the value of additional survey points. Section 4.2 assesses the value of potential survey locations u . Section 4.3 examines a sub-region of the study site and puts into a spatial context some of the results of earlier sections.

4.1 Model Validation

One may determine how well simulated terrains compare to reality in terms of elevation and flood extent. Surface **R**, introduced in section 3.1 represents reality, as it was kriged from the full original data set r . Each of the 3120 **C** surfaces was subtracted from **R**, yielding a mean volumetric difference between the **C** surfaces and **R** of $56\,497\text{ m}^3$ ($s^2 = 75\,760$), with a minimum of 95 m^3 and maximum of $230,887\text{ m}^3$. These figures compare favorably with respect to **R**'s total volume of approximately 1.5 million m^3 . The mean difference in surface elevation between **R** and each of the 3120 **C** surfaces is 0.105 m ($s^2 = 0.14$), the minimum 0.0010 m , and the maximum 0.428 m . As before, the performance of the procedure in simulating **C** is adequate

given that the maximum height in the study area is 4.6 m; and that the mean value of 0.105 m is within the 0.15 m error range for r .

Elevation is also affected by the fact that conditionally simulated surfaces, as a rule, are rougher than kriged terrains. The kriged map, while providing the ‘best’ estimate of the elevation at any particular location will, because of the interpolation procedure, produce topography with much spatial dependence. Therefore, the smoothly varying surface of a kriged map may not adequately describe how the flood state of a given cell is affected by the elevation of its neighboring cells. In the example, the kriged map **A** has a Moran’s I of 0.92 (a measure of spatial autocorrelation²), while **B** and **C** have a mean of 0.77, indicating rougher surfaces. As noted in section 3.3, this roughness is critical given the importance of the height of neighboring cells to flooding in a given cell. Similarly, one expects the mean difference between surface **A** and either of series **B** and **C** to tend towards zero over very large numbers of realizations. A large difference would mean that the simulated surfaces are not a good approximation of reality.

The second test of simulated terrains against reality is to compare flood extent. The Federal Emergency Management Agency (FEMA) prepares Flood Insurance Rate Maps that depict spatial extent of flood hazards. Of particular importance are areas: X, those with less than a 0.2% chance per annum of flooding (i.e., areas that would be inundated by a flood with a return period of 500 years); AE, regions with greater than 1% chance of flooding per annum (i.e., a 100-year flood); and VE, areas of velocity hazard (e.g., storm surge) and a greater than 1% chance of flooding per annum. Figure 4 details the extent of FEMA classes.

Insert Figure 4 here

In order to compare flooding in the simulated terrains and the FEMA maps, it is necessary to determine the extent of flooding in the former. Given the Monte Carlo basis for the Bayesian procedure, it is possible to create probabilistic flood maps. The following procedure is repeated once for each of ten flood heights (h) ranging from 0.3 m to 3.0 m. First, each of the 3120 **C** series surfaces is flooded to a given height (as described in section 3.4). Second, each of these flooded terrains is converted into a Boolean mask depicting the flood state of each cell in that terrain at that flood height. Third, a composite flood map is then created by overlaying these 3120 Boolean images in Idrisi and rescaling the result from zero to one. The net result is ten different flood probability maps, each the result of flooding the 3120 **C** terrains to a given flood height.

Each of these ten composite flood maps can be treated as a probabilistic statement of flooding in Point of Pines for a given flood height. Cells take a value, termed Pf for *probability of flooding*, that ranges from zero to one. A zero value for a given cell indicates that none of the 3120 Boolean masks contributing to the composite flood map has flooding in that cell. A value of one indicates the highest level of agreement between the masks whether the cell in question is flooded at a given flood height. It is important to note that Pf is a measure of agreement on flooding between terrains, while probability in FEMA maps is based on historic, meteorological, hydrologic, and hydraulic data. These two kinds of probability cannot therefore be compared. It is desirable to compare flooding in **C** terrains to flooding in reality, however, and the FEMA maps are a good source of data on the latter. It is possible to compare how the flood extents for FEMA classes compare to flood extents in simulated terrains.

Table 1 demonstrates that simulated flooding corresponds with FEMA flood zones AE and VE. For each flood height h there exists a series of flood extents that vary in size with

² A better means of measuring spatial autocorrelation in these maps would be to use the variograms. Given computational restraints, the simpler Moran’s I is used here to illustrate a general conclusion.

probability of occurrence in the simulations (Pf). A value of $Pf = 0.01$ denotes the broadest possible flood extent, one that includes every cell in the composite map that has even the smallest chance of inundation. A $Pf = 0.01$ therefore results in the largest, if least likely, floods. Due to their large size, these floods spill over into FEMA zone X. As a result, an average of 78% of simulated flooding occurs in FEMA zones AE and VE across all heights of h and 22% (incorrectly) occurs in zone X. At the other extreme, a Pf of 0.99 defines floods that include only cells most likely to flood, and therefore 98% of this simulated flooding occurs in FEMA flood zones. In fact, when $Pf = 0.99$, all flooding at heights of 2.1 m or less is correctly classified as being in FEMA zones AE and VE.

Insert Table 1 here

By increasing Pf , locational specificity of flood occurrence becomes increasingly certain, but at the risk of underestimating flood extent. At a flood height of 1.5 m and Pf of 0.90 in Table 1, for instance, 92% of simulated flooding is classified correctly while a Pf of 0.10 yields an accuracy of 82%. One is therefore tempted to use the higher Pf to gain greater classification accuracy. This accuracy comes at a cost, however, as illustrated by Figure 5, in which the trade-off between area of simulated flooding correctly classified (Y-axis) and the flooding probability Pf (X-axis), is presented. To continue the example of a 1.5 m flood height, a $Pf = 0.10$ yields approximately 130,000 m² of correctly classified simulated flooding while at $Pf = 0.90$ there is only 230 m².

Insert Figure 5 here

Table 1 and Figure 5 illustrate the fundamental trade-off in certainty between locational accuracy and flood extent. Even without access to FEMA flood data, a decision maker understands this trade-off is present when using probabilistic flood maps. If one is risk-adverse in terms flood extent, then a low Pf in the flood maps will indicate the largest possible flood area. Conversely, if one wants to determine which cells are most likely to be inundated at a given height h , then a high Pf will highlight these cells at the risk of underestimating their number.

4.2 General Bayesian Analysis

In this section, the general Bayesian analysis introduced in section 2.1 is evaluated for the Point of Pines study area. The results reveal several issues specific to the study site that require spatially explicit examination with GIS, which is undertaken in the next section (4.3).

The value of the information about flood patterns provided by additional locations u is obtained by comparing the extent of flooding in the simulated terrain sets **B** and **C**. Calculating the value of information of the additional points u can be obtained by reconfiguring Equation 2 as:

$$V(U) = |E(E^*(x, u) | x) - E^*(x)| \quad (4)$$

where $V(U)$ is the value of the extra locations expressed as the difference between expected flood extent with the additional points $E(E^*(x, u) | x)$ and those under current knowledge $E^*(x)$. The decision maker acquires u when the value of $V(U)$ is greater than costs ($C(U)$) of acquiring u . The value of $V(U)$ may be calculated as the loss function (damages due to flooding) expressed in Equation 1 as $L[\phi, \delta(x)]$ and reinterpreted as elevation-dependent flooding in Equations 2 and 3:

$$V(U) = L_U[D(h), u | x] - L_X[D(h), x] \quad (5)$$

In this case, $V(U)$ is the absolute difference between losses due to flooding associated with additional knowledge, L_U (i.e., flooding in **C**), and flood losses under current knowledge, L_X (i.e., flooding in **B**).

As the analysis presented here is general in scope, $D(h)$ in Equation 5 approximates flood damage for the study site as a whole. In reality, hydrological engineers construct flood stage damage estimates that assess damage as a function of a spatially detailed understanding of land use and flood height at specific locations. Total damages for the area would be the aggregation of those land use and location-specific damage estimates. Here $D(h)$ is considered for the entire study site in terms of $D(h) = D_B + D_B(ha)$. The first term of this equation, base damage D_B , approximates damage to the study site as a whole with areal flood extent (in m^2) at a given flood height h . The second term, $D_B(ha)$, reflects that damage in any particular location increases with flood height h . Constant a determines the extent to which h modifies $D(h)$.

Using the generalized damage function with the example topography, Table 2 demonstrates the difference in flooding damage between simulations **B** and **C** for ten flood heights (h ranges from 0.3 m to 3.0 m). Simulations are grouped into three intervals according to the number of additional points n_u from which **C** is derived, denoted u_{200} ($n_u = 25$ to 200), u_{400} ($n_u = 225$ to 400), and u_{600} ($n_u = 425$ to 600). Combinations of h , a , and n_u where $V(U) \geq C(U)$, for a hypothetical situation where $C(U)$ to survey u_{200} , u_{400} , and u_{600} is 2000, 4000, and 6000 respectively, are shown in bold type in Table 2.

Insert Table 2 here

The decision maker can come to three conclusions concerning h , n_u , and a as a result of the general Bayesian analysis in this example. First, when $h > 2.3$ m the decision maker acquires u more often than not, while at $h < 0.9$ m the decision maker rarely chooses to acquire u . Second, in addition to directly contributing to the magnitude of $C(U)$, n_u has decreasing marginal utility in that $V(U) \geq C(U)$ when $a = 0$ for 50% of flood heights for u_{200} , 30% for u_{400} , and 20% for u_{600} . Third, a modifies the role of h and n_u in determining whether $V(U) \geq C(U)$. When $a = 0.6$ (Table 2), the decision maker solidifies decisions for low and high h , and the decreasing marginal utility of n_u is attenuated as $V(U) \geq C(U)$ for 70% of all cases.

The decision maker finds it difficult, however, to find a consistent relationship between $V(U)$ and $C(U)$ in the middle flood heights (i.e., $0.9 \text{ m} \leq h \leq 2.1 \text{ m}$). Figure 6 illustrates the effect of varying n_u at a flood height of 1.8 m. Each column indicates the number of **C** realizations that have a flood extent falling within a given 7500 m^2 interval. Solid columns indicate 390 **C** terrains based on a n_u of 75, 100, and 125 (denoted u_{100}) and outlined columns indicate a second set of 390 terrains where $n_u = 550, 575, \text{ and } 600$ (denoted u_{600}). The bulk of terrains (as indicated by frequency on the Y-axis) have flood extents of roughly 50 000 to 70 000 m^2 regardless of n_u . Of particular interest is the bimodality of u_{600} compared to the single mode of u_{100} . Approximately 20% of the u_{600} terrains have flood extents in the 110 000 m^2 range. This second peak complicates the derivation of $V(U)$ as a function of n_u given a lack of an evident, normal distribution of flood extents.

Insert Figure 6 here

4.3 Spatially Localized Analysis

The analysis thus far has established several relationships between $V(U)$ and $C(U)$ but also raised three issues for this particular study site. One, as illustrated in section 4.1, there is a probabilistic tradeoff in certainty between location and quantity. Two, the value of $V(U)$ as a function of h is unclear at mid flood heights. Three, the size of n_u affects flood damage estimates. These issues

raise an additional question as to where the additional survey locations u should be located. This reflects the importance of accounting for topographical discontinuities in surface interpolation (Kyriakidis et al. 1999), and the way floods manifest through the terrain.

One means of identifying good locations for additional points is by referring to the kriging variance (σ_e^2). Figure 7 is an isopleth map of variance from **A**, rescaled from 0 to 100. In general, kriging variance is a function of spatial correlation. It decreases with higher sampling density, which holds true here considering the location of x (inset) and the area of highest variance indicated by an ellipse in the figure. The variance also reflects where spatial correlation is weak due to a particular geometric configuration, such as discontinuous terrain. The variance surface describes the effects of the sampling scheme of x relative to γ and thereby identifies where additional points u should be placed to augment x and reduce σ_e^2 .

Insert Figure 7 here

The decision maker can combine knowledge imparted from the kriging variance with that from probabilistic flood maps in order to better identify suitable survey locations. Figures 8a and 8b contain probability (Pf) isoline maps for the study site's north central region at 1.5 m and 1.8 m flood heights. As noted in section 4.2, the decision maker faces difficulty in determining $V(U)$ at these flood heights. This is especially so when the effects of n_u are considered, so figures 8a and 8b contain two maps apiece, one created from **C** terrains based on $n_u = 100$ and the other $n_u = 600$. For the following discussion, road features overlay the probability images.

Insert Figures 8a and 8b here

These figures illustrate two characteristics of flooding in the simulated images that bear on the decision maker's analysis. First, the two maps where $n_u = 100$ have contour spacing that is more regular than for the two maps where $n_u = 600$. Second, the orientation of flooding isolines in the $n_u = 600$ maps at lower values of Pf appears to be influenced by roads. Three directions are of interest in determining the validity of these initial impressions. First, the shoreline describes a 100 degree angle, termed θ , which is the northern periphery of floods (north = 0 degrees). The bulk of isolines close to the ocean run parallel to θ , although this proportion declines when $Pf < 0.5$. Second, α denotes the 20 degree orientation of study site topography, major roads, and the variogram anisotropy bearing. Isolines on the east and west flood peripheries are oriented along α . Third, minor roads in the sub-region are oriented at a 135 degree angle denoted β , along which run a proportion of low probability isolines (when $Pf < 0.3$). Black circles in figures 8a and 8b mark key points where this is particularly apparent. Moreover, the degree of orientation between low probability flood isolines and minor roads appears greater in the maps where $n_u = 600$.

The decision maker can obtain a better grasp of flood orientation by considering flood probability as a three dimensional surface. The first derivative of this surface is approximated by slope (S_p), a measure of the rate of change in probability, and aspect (A_p), the direction of maximum slope. With S_p and A_p , the decision maker may determine the orientation of flooding. Table 3 details the proportion of cells with A_p perpendicular to the key angles noted above within 5 or 10 degrees. The three final rows in particular demonstrate that the probability surfaces based on a larger n_u have a greater proportion of isolines oriented along minor roads. The decision maker surmises that flooding may be affected by minor roads in this sub-region.

Insert Table 3 here

Table 3 does not imply that simulations with larger numbers of additional points are more realistic. As noted in section 3.3, no information from reality except the original survey locations x is introduced into the estimated topography of Point of Pines. It is important to

consider the fashion in which the conditional simulation algorithm operates. It selects a random location and krigs an elevation value and kriging variance. The simulated value for that location is then randomly selected from a normal distribution with a mean and variance equivalent to the kriged value. This cell-by-cell process is repeated until the surface grid is filled. All initial input data and previously simulated locations are used to simulate later locations in order to maintain correspondence to the variogram.

The sequential, additive nature of the simulation algorithm explains how roads can be important to understanding flooding. As a subset of original samples r was taken in the area of minor roads, a small number of these locations make their way into x and thereby into **B** and **C**. The linearity of roads imparted to a given simulation by these points is not generally evident because it runs counter to kriging anisotropy. As n_u grows, however, increasing numbers of locations u from **B** are constrained in **C** and there is a small probability that critical initial cells simulated in **C** will lie along β and thereby preserve road linearity in a small subset of realizations. This trend weakens as kriging variance increases and simulated cells grow less dependent on x or u .

A complementary trend is that flooding is an asymmetric spatial process since high simulated values do not have the same effect as low ones for any given cell. Since a road acts as a linear barrier against flooding, any or all of its constituent cells can be higher in elevation than flood height without deleterious effects. The reverse does not hold, however, since a single low cell will expose the area protected by the road to flooding regardless of the height of neighboring cells. This fact goes to the heart of the description of the Monte Carlo process given in section 3.3, on the importance of conditional simulation to creating spatially contiguous cells that vary in height. Given the sequential nature of conditional simulation, having fewer initial points from which to simulate locations results in simulated values closer to the mean surface elevation. With increasingly large numbers of u , it is more likely that some location with a relatively low elevation will be introduced near a road before the cells in the surface are simulated. This low-valued cell influences nearby simulated locations and has a net affect of creating depressions in roads and reducing their effectiveness as barriers against flooding.

When taken together, kriging variance and the impact of roads create localized floods. These floods lie at the heart of issues raised in section 4.1, the tradeoff between location and quantity, and in section 4.2, how $V(U)$ is affected by both middle flood heights and n_u . Consider the bimodality raised previously by Figure 6. When $n_u = 600$, a subset of **C** (indicated by low Pf) have floods that are somewhat separated from the main body of high Pf floods as a result of flooding being guided and blocked by roads. These separate, localized floods create bimodality in an area flooded when $n_u = 600$ and therefore affect $V(U)$.

Localized floods also complicate the relationship between h and $V(U)$ because at a given flood height there is an irregular flood extent upon which to base $D(h)$. The problem exists at mid flood heights since lower flood heights rarely reach the roads and higher floods ignore them. Flood localization also makes it necessary to focus on the interplay between location and quantity as a function of Pf in spatially discrete regions of the study site. If the decision maker is satisfied with assessing only high Pf floods then location becomes relatively fixed, quantity is easily measured, and localization is less of an issue. If instead low Pf floods are of interest, then a more tailored set of u is necessary to offset flood localization.

As noted above, simulated topography based on larger numbers of additional points u does not necessarily better approximate flooding. Figures 8a and 8b agree that high Pf cells are coincident in most simulated terrains regardless of n_u . Similarly, slope (S_p) indicates that Pf is

smoothly varying for high Pf isolines; discontinuity in slope occurs only for lower Pf values. The decision maker cannot therefore make decisions about flooding in reality based solely on the simulated behavior of low Pf floods.

The decision maker may safely decide, however, to survey additional locations with a spatially stratified sampling frame that accommodates anomalies highlighted by the Bayesian procedure. Once the quantity of additional locations is approximated by the general, study site wide analysis in section 4.2, the decision maker can use spatially localized analysis to further guide sample selection. In particular, locations should be chosen in regions of simulated localized flooding and high kriging variance. In addition to considering the direct contribution of n_u to $C(U)$, as in section 4.2, the decision maker should iteratively explore $V(U)$ as a function of key parameters such as n_u and h at different analytical scales to gain a contextual understanding of the potential value of additional survey locations.

5 Conclusion

This study illustrates the application of Bayesian theory to an explicitly spatial setting and complements current work in decision making under uncertainty. In particular, this paper demonstrates how a joint GIS-geostatistics framework allows a decision maker to assess the value of additional information before its acquisition in order to better understand the spatiality of flooding. A detailed exploration of the localized area with the GIS, prompted by specific issues raised by the nested Monte Carlo analysis, provided information that may not have been apparent if either technique were used alone.

A key area of further exploration is use of spatially discrete damage functions based on flood elevations and land uses at specific locations. An allied extension is the introduction of structural flood policy responses, such as sea walls, and the assessment of their impact with the Bayesian procedure. Tying this analysis to a process model of flooding (as opposed to the sunken valley approach used here) would also be of benefit, as would evaluating the role of error propagation in the procedure to provide a deeper understanding of uncertainty. Finally, as the interoperability and power of GIS and geostatistical packages grows, the potential for the kind of research described here increases as well, allowing geographical modelers to leverage the strengths of these two fields.

Acknowledgements

This work is supported in part by NOAA grant NA 36GP0520 and National Science Foundation Grant Number 9521914 through the Carnegie Mellon University Center for Integrated Study of the Human Dimensions of Global Change. The authors thank the reviewers and editor for their comments, all of which made for a better paper. Responsibility for any errors or omissions is solely that of the authors.

Figures

Figure 1 – Methodology for Bayesian assessment of the value of information (use of γ in step 2a and step 2c is implied).

Figure 2 – Study site elevation contours (meters) with road features (lower inset) and guide map (upper inset)

Figure 3 – Known sample locations x

Figure 4 – FEMA flood classes X, AE, and VE

Figure 5 – Cumulative area of correctly classified flood area as a function of flood probability (P_f) for varying flood heights

Figure 6 - Frequency of flood extents in simulated terrains at the 1.8 m flood height for surfaces simulated with 100 and 600 additional points

Figure 7 – Kriging variance for \mathbf{A} rescaled from 0 to 100 and inset with known sample points x

Figure 8a – Probability of flooding for flood heights of 1.5 m over sets of simulated surfaces created with 100 and 600 additional points. Angles θ , α and β are indicated, as are key locations of interest and roads

Figure 8b – Probability of flooding for flood heights of 1.8 m over sets of simulated surfaces created with 100 and 600 additional points. Angles θ , α and β are indicated, as are key locations of interest and roads

Literature Cited

- Anselin, L. and A. Getis (1992). "Spatial statistical analysis and geographical information systems." *Annals of Regional Science* 26, 19-33.
- Berger, J. O. (1986). *Statistical Decision Theory and Bayesian Analysis*. New York, Springer-Verlag.
- Burrough, P. and R. McDonnell (1998). *Principles of Geographic Information Systems*. New York, Oxford.
- Chrisman, N. (1991). "The error component in spatial data." *Geographic Information Systems: Principles and Applications*. edited by Maguire, D. J., M. F. Goodchild and D. W. Rhine. Harlow, UK, Longman Scientific and Technical. Volume One: 165-174.
- Cyert, R. M. and I. DeGroot (1987). *Bayesian Analysis and Uncertainty in Economic Theory*. Totowa, NJ, Rowman & Littlefield.
- Deutsch, C. V. and A. G. Journel (1992). *GSLIB: Geostatistical Software Library and User's Guide*. New York, Oxford University Press.
- Dixon, T. H. (1995). *SAR Interferometry and Surface Change Detection*. Miami, FL, University of Miami.
- Eastman, R. (1999). *Guide to GIS and Image Processing*. Worcester, MA, Clark University.
- Goodchild, M. F., B. P. Buttenfield and J. Wood (1994). "Introduction to visualizing data quality." *Visualization in Geographical Information Systems*. edited by Hearshaw, H. M. and D. J. Unwin. New York, John Wiley and Sons: 141-149.
- Heuvelink, G. (1993). *Error Propagation in Quantitative Spatial Modelling: Applications in Geographical Information Systems*. Amsterdam, Koninklijk Nederlands Aardrijkskundig Genootschap.
- Hill, J. M., L. A. Graham, R. J. Henry, D. M. Cotter, A. Ding and D. Young (2000). "Wide-area topographic mapping and applications using airborne Light Detection and Ranging (LIDAR) technology." *Photogrammetric Engineering and Remote Sensing* 66 8, 908-914.
- Husain, T. (1990). "Hydrologic uncertainty measure and network design." *Water Resources Bulletin* 25 3, 527-534.
- Isaaks, E. H. and R. M. Srivastava (1989). *Applied Geostatistics*. New York, Oxford University Press.
- Journel, A. G. (1996). "Modelling uncertainty and spatial dependence: Stochastic imaging." *International Journal of Geographical Information Systems* 10 5, 517-522.

- Kyriakidis, P. C., A. M. Shortridge and M. F. Goodchild (1999). "Geostatistics for conflation and accuracy assessment of digital elevation models." *International Journal of Geographical Information Science* 13 7, 677-707.
- Leatherman, S. P. (1992). "Sea level rise: Implications and responses." *Global Climate Change: Implications, Challenges, and Mitigation Measures*. edited by Majundar, L. S., B. Kalkstein, E. W. Yarnal and L. M. Rosenfeld. Philadelphia, PA, Pennsylvania Academy of Science: 256-263.
- Melching, C. S. and S. Anmangandla (1992). "Improved first-order uncertainty method for water-quality modeling." *Journal of Environmental Engineering* 118 5, 791-805.
- Oliver, M. and R. Webster (1986). "Semi-variograms for modelling the spatial pattern of landform and soil properties." *Earth Surface Processes and Landforms* 11, 491-504.
- Ostroff, G. and S. Tucker (1992). "Using a GIS to analyze the effects of sea level rise." *Global Climate Change: Implications, Challenges, and Mitigation Measures*. edited by Majundar, L. S., B. Kalkstein, E. W. Yarnal and L. M. Rosenfeld. Philadelphia, PA, Pennsylvania Academy of Science: 264-273.
- Panatier, Y. (1996). *VarioWin: Software for Spatial Data Analysis in 2D*. New York, Springer-Verlag.
- Pebesma, E. J. (1996). *GSTAT*. Amsterdam, Netherlands Centre for Geo-ecological Research.
- Ratick, S. J., A. Solow, J. Eastman, W. Jin and J. Hong (1994). *A Method for Incorporating Topographic Uncertainty in the Management of Flood Effects Associated with Changing Storm Climate*. Worcester, MA, George Perkins Marsh Institute.
- Rosbjerg, D. and H. Madsen (1995). "Uncertainty measures of regional flood frequency estimators." *Journal of Hydrology* 167, 209-224.
- Solow, A. R. and S. J. Ratick (1994). "Conditional simulation and the value of information." *Geostatistics for the Next Century*. edited by Simitrakopoulos, R. Dordrecht, Netherlands, Kluwer Academic Publishers: 209-217.
- USACE (1994). *Topographic Surveying (EM 1110-1-1005)*. Washington, DC, United States Army Corps of Engineers.
- USACE (1997). *Practical Aspects of Applying Geostatistics at Hazardous, Toxic, and Radioactive Waste Sites (ETL 1110-1-175)*. Washington, DC, United States Army Corps of Engineers.
- Wigley, T. M. L. and S. C. B. Raper (1992). "Implications for climate change and sea-level rise of revised IPCC emissions scenarios." *Nature* 357, 293-300.

Figure 1 – Methodology for Bayesian assessment of the value of information (use of γ in step 2a and step 2c is implied).

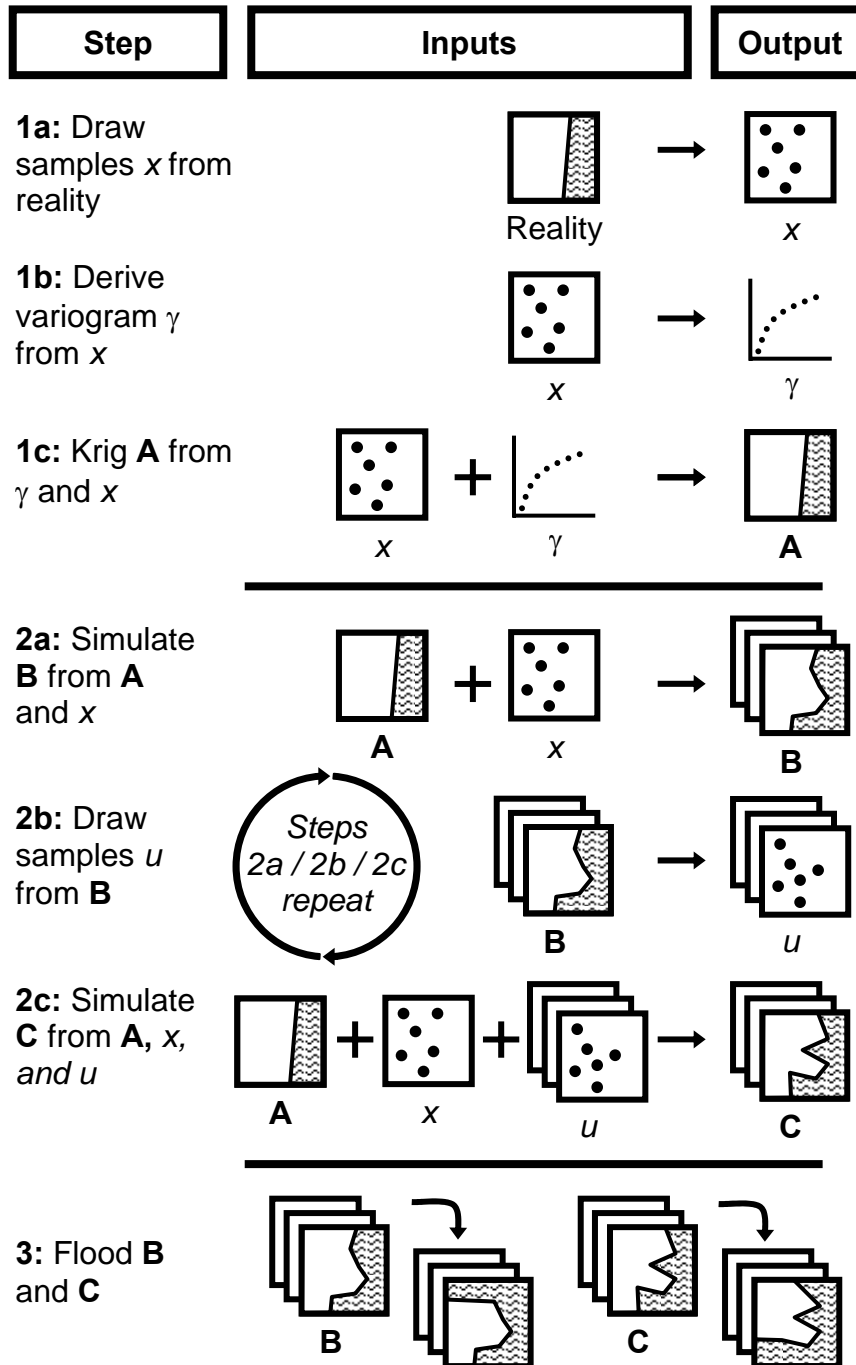


Figure 2 – Study site elevation contours (meters) with road features (lower inset) and guide map (upper inset)

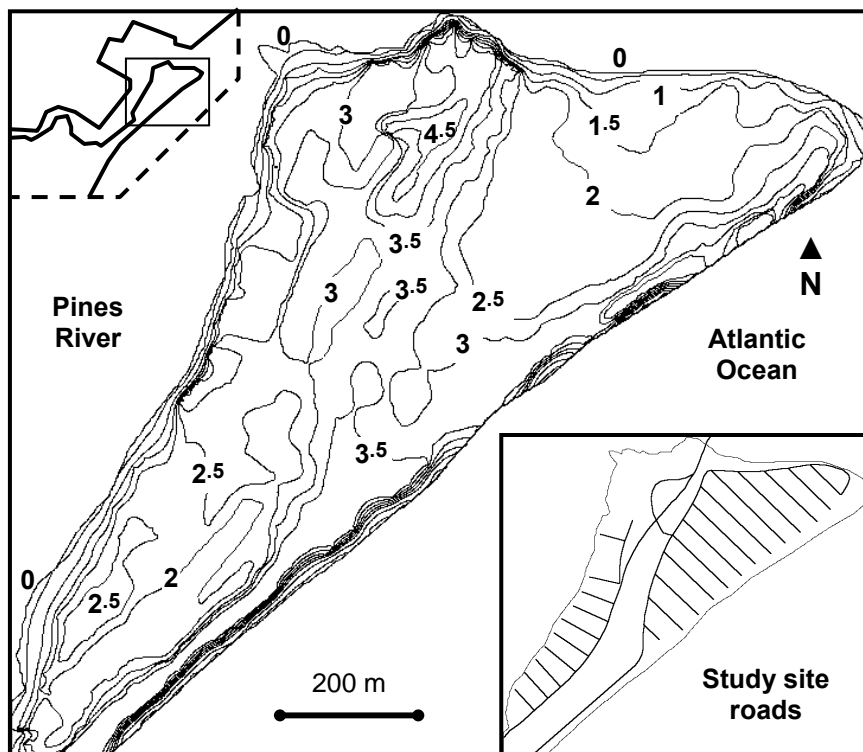


Figure 3 – Known sample locations x

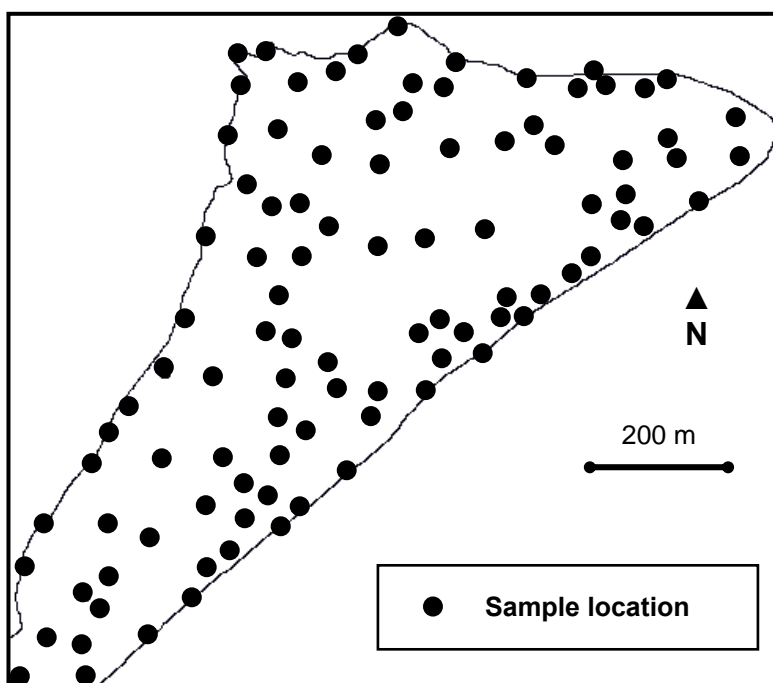


Figure 4 – FEMA flood classes X, AE, and VE

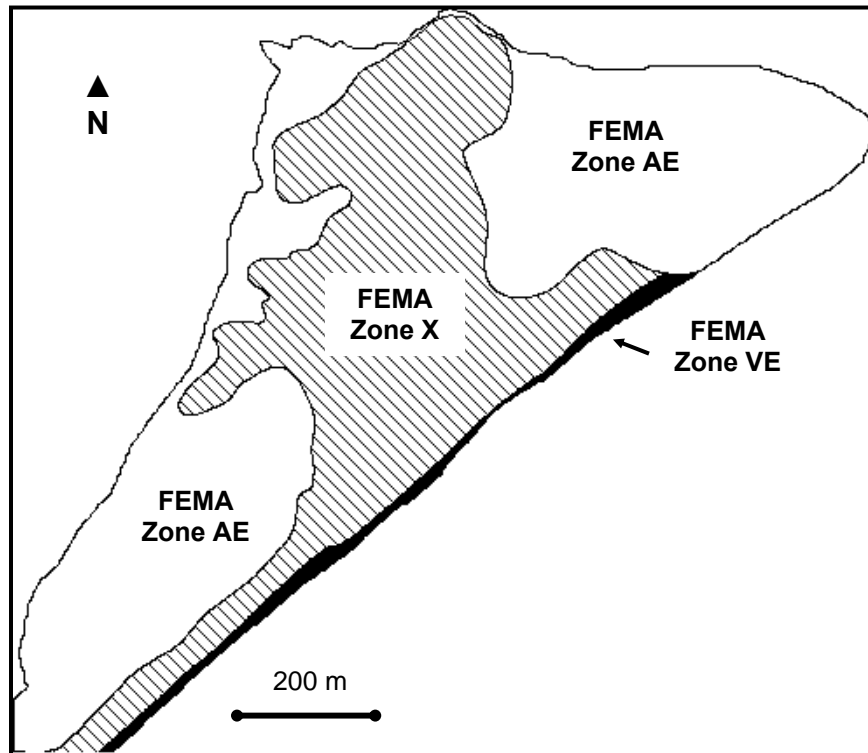


Figure 5 – Cumulative area of correctly classified flood area as a function of flood probability (P_f) for varying flood heights

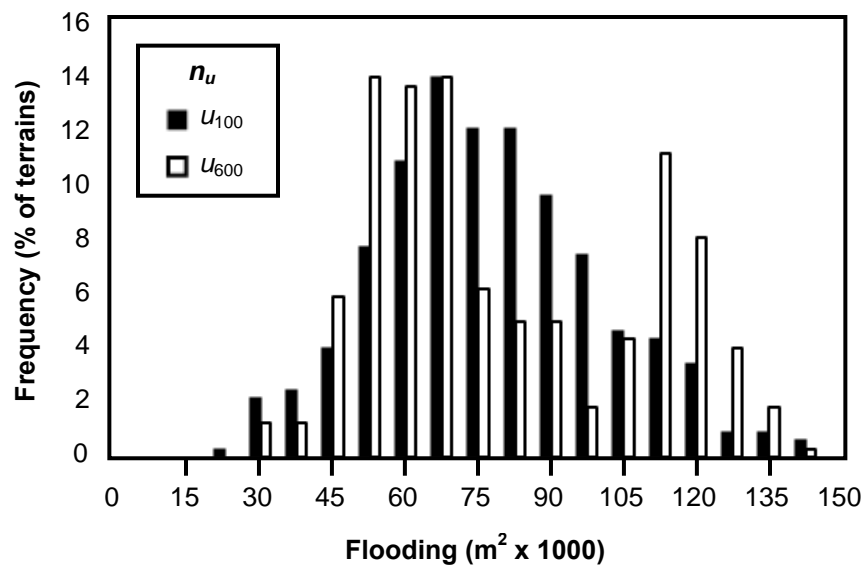


Figure 6 - Frequency of flood extents in simulated terrains at the 1.8 m flood height for surfaces simulated with 100 and 600 additional points

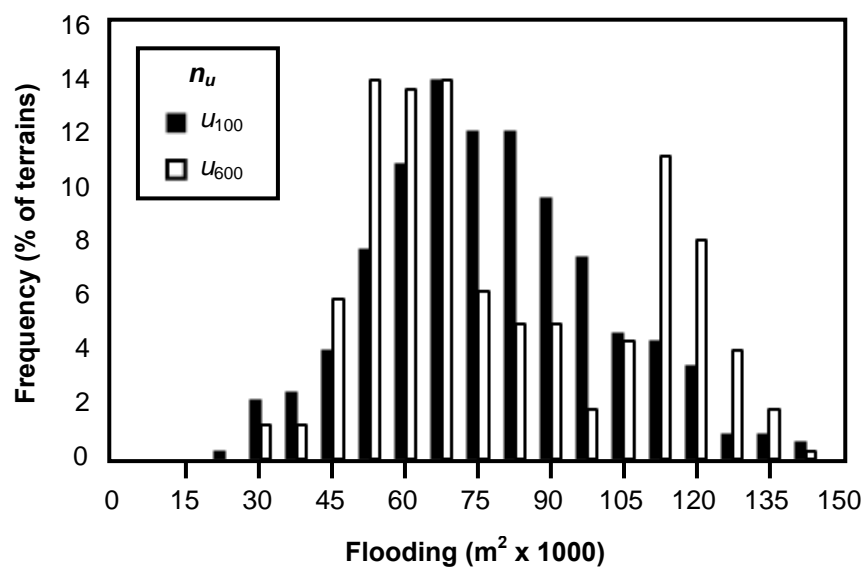


Figure 7 - Kriging variance for \mathbf{A} rescaled from 0 to 100 and inset with known sample points x

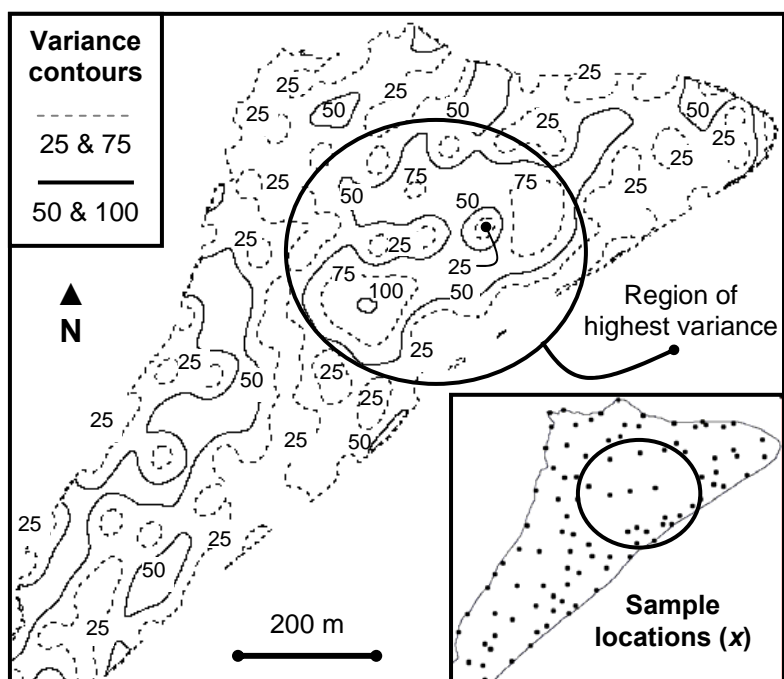


Figure 8a – Probability of flooding for flood heights of 1.5 m over sets of simulated surfaces created with 100 and 600 additional points. Angles θ , α and β are indicated, as are key locations of interest and roads

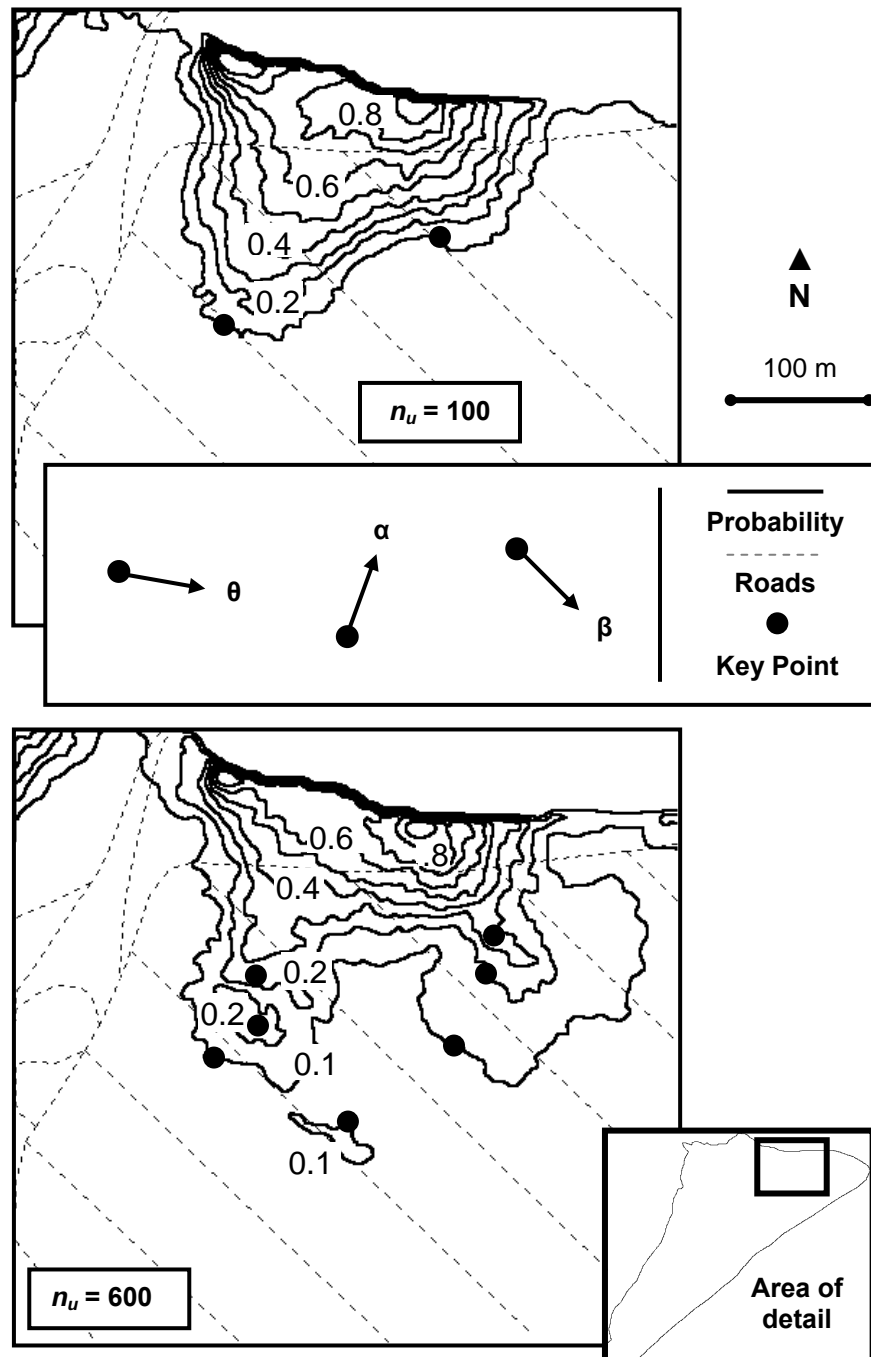


Figure 8b – Probability of flooding for flood heights of 1.8 m over sets of simulated surfaces created with 100 and 600 additional points. Angles θ , α and β are indicated, as are key locations of interest and roads

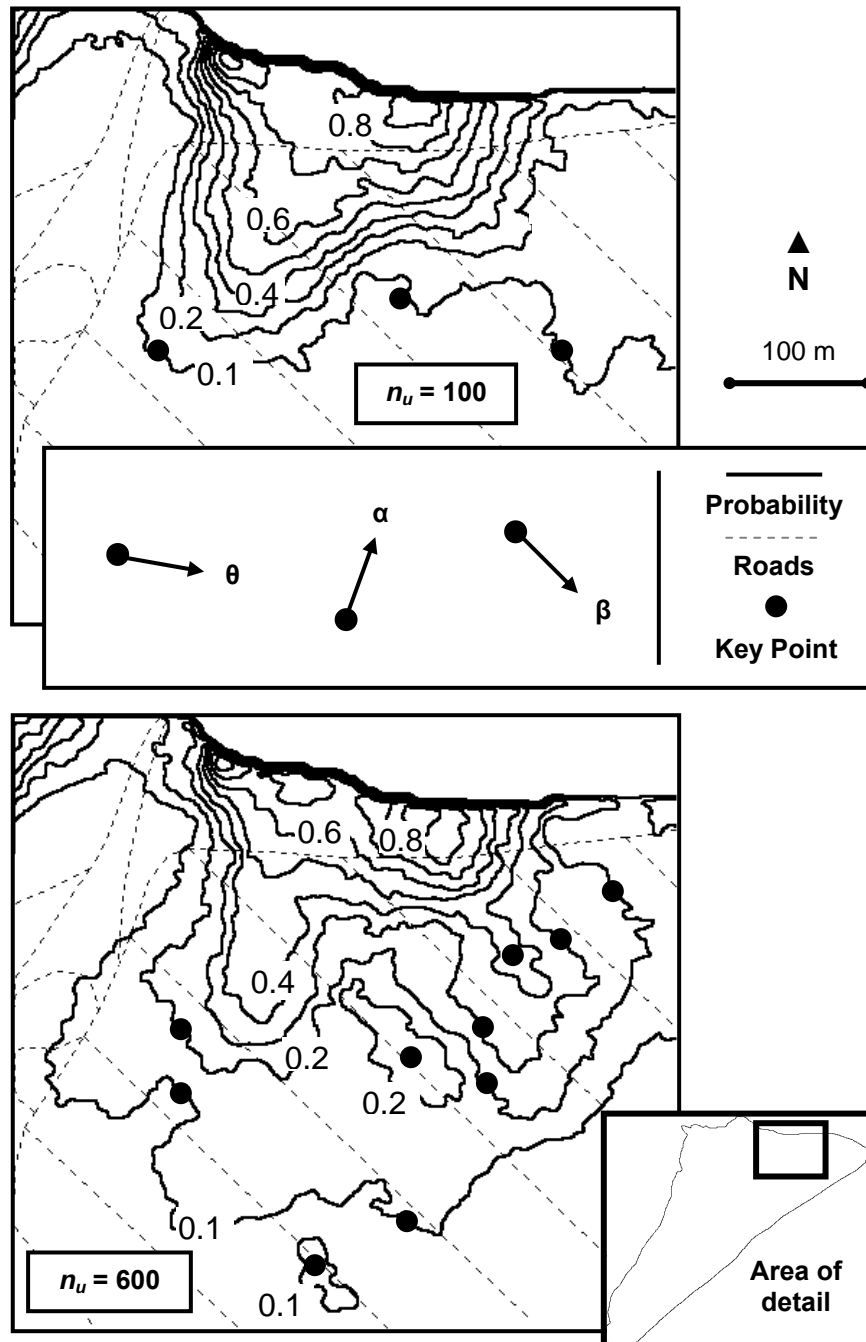


TABLE 1

Percentage of correctly classified simulated flood cells (i.e., cells in FEMA flood zones AE & VE) by flood height and probability of occurrence in the simulations

Probability (P_f)	Flood height (m)										Mean %
	0.3	0.6	0.9	1.2	1.5	1.8	2.1	2.4	2.7	3.0	
0.01	78	79	80	80	79	78	77	76	76	76	78
0.10	77	79	80	80	82	84	81	78	77	76	79
0.20	80	81	87	89	87	87	88	82	78	77	84
0.30	80	81	81	87	89	88	90	89	82	78	85
0.40	83	83	83	82	88	90	90	92	87	81	86
0.50	86	85	85	84	84	87	89	92	92	86	87
0.60	90	86	86	84	84	84	86	89	93	90	87
0.70	92	91	89	88	86	84	84	84	90	94	88
0.80	89	93	92	89	88	86	84	83	84	90	88
0.90	100	100	100	100	92	91	88	86	83	84	92
0.99	100	100	100	100	100	100	100	98	90	88	98

TABLE 2

Value of u for combinations of b and n_u for $a = 0$ and $a = 0.6$

Flood stage (m)	$V(U)$ when $a = 0$			$V(U)$ when $a = 0.6$		
	u_{200}	u_{400}	u_{600}	u_{200}	u_{400}	u_{600}
0.3	1736	1479	1251	2048	1745	1476
0.6	1685	1487	1429	2292	2022	1943
0.9	4118	4083	4296	6341	6288	6617
1.2	835	300	1111	1436	516	1912
1.5	3044	4659	7117	5784	8851	13522
1.8	1790	780	2800	3723	1622	5824
2.1	534	3653	2417	1207	8256	5462
2.3	3874	2008	2857	9454	4899	6971
2.7	8167	6432	6410	21398	16851	16794
3.0	3785	2495	2364	10598	6985	6621

Note: combinations of b and n_u **bolded** where $V(U) \geq C(U)$

TABLE 3
Correspondence between aspect (A_p) and angles θ , α and β for margins of 5° & 10°

Angle/Bearing	Proportion in 5° margin				Proportion in 10° margin			
	Flood height = 1.5 m		Flood height = 1.8 m		Flood height = 1.5 m		Flood height = 1.8 m	
	$n_u=100$	$n_u=600$	$n_u=100$	$n_u=600$	$n_u=100$	$n_u=600$	$n_u=100$	$n_u=600$
Proportions of cells with A_p perpendicular (\perp) to θ , α and β								
$A_p \perp \theta$ (10°)	0.00	0.02	0.00	0.02	0.00	0.03	0.00	0.02
$A_p \perp \theta$ (190°)	0.33	0.36	0.41	0.29	0.40	0.42	0.47	0.37
$A_p \perp \alpha$ (110°)	0.26	0.21	0.24	0.20	0.24	0.20	0.20	0.18
$A_p \perp \alpha$ (290°)	0.19	0.09	0.14	0.16	0.17	0.08	0.14	0.15
$A_p \perp \beta$ (45°)	0.00	0.09	0.02	0.09	0.00	0.07	0.01	0.08
$A_p \perp \beta$ (225°)	0.21	0.22	0.19	0.24	0.19	0.20	0.18	0.21
Proportions of cells with A_p perpendicular (\perp) to θ , α and β								
$A_p \perp \theta$	0.33	0.38	0.41	0.31	0.40	0.45	0.47	0.39
$A_p \perp \alpha$	0.45	0.30	0.38	0.36	0.41	0.28	0.34	0.33
$A_p \perp \beta$	0.21	0.32	0.21	0.33	0.19	0.28	0.19	0.29
Proportion of cells in images $n_u = 100$ divided by those where $n_u = 600$								
$A_p \perp \theta$	0.87		1.30		0.90		1.22	
$A_p \perp \alpha$	1.50		1.05		1.46		1.02	
$A_p \perp \beta$	0.68		0.64		0.69		0.67	